

Chapter 2

Distinct Diameter Dependence of Redox Property for Armchair, Zigzag Single-walled, and Double-walled Carbon Nanotubes

Wenming Sun, Yuxiang Bu and Yixuan Wang

Abstract Multiscale density functional theories (DFTB, PBE, and M06-2X) were used to investigate redox properties, such as ionization potentials (IP), electron affinities (EA), electronegativities (χ), and Fermi levels (E_F) for infinite armchair single-walled carbon nanotubes (SWNT) (n,n) ($n=3-16$), zigzag SWNT (n,0) ($n=5-16$), as well as double-walled carbon nanotubes (DWNT) (n,n)@(n+5, n+5) ($n=3, 5$ and 6). These properties show strong and different diameter dependence. With increasing diameter, IPs of armchair SWNTs (n,n) decrease monotonically, while EAs increase monotonically. Although IPs of zigzag SWNTs (n,0) also generally decrease, there is an increase occurring just after $(3k, 0)$ ($k=2, 3, 4$, and 5) and shows a group behavior, in which every three neighbourhood $(3k, 0)$, $(3k-1, 0)$ and $(3k-2, 0)$ form a group. However, opposite to the armchair SWNTs, the EAs of zigzag SWNTs decrease rapidly with increasing diameter till $(11, 0)$ and then gently increase. EAs of the zigzag SWNTs also exhibit a group behavior, yet are not synchronous with IPs. With increasing diameter, the IPs and EAs of both the armchair and zigzag SWNTs approach to approximately 4.7 and 3.9 eV. For the armchair SWNTs electronegativity (χ) and Fermi level ($-E_F$) change very slightly with diameter, while for the zigzag they decrease rapidly till $(9, 0)$ and then gently oscillate to the similar levels to those of the armchair. The IPs and EAs for (n,n)@(n+5, n+5) DWNTs have the same trend as armchair SWNTs. It was also found that these DWNTs characterize better redox properties than their constituents. These interesting findings are important for redox chemistry based on CNTs and may offer a new strategy for separation of CNTs. The biomedical implication of SWNT, C_{60} and $Li@C_{60}$ was also discussed. Similar to $Li@C_{60}$, the binding and HOMO analysis shows that SWNT may also be able to well protect DNA bases from radiation.

Submitted to the book "Design and Applications of Nanomaterials for Devices and Sensors" edited by J. Seminario, 2013

Y. Bu (✉) · W. Sun

The Center for Modeling & Simulation Chemistry, Institute of Theoretical Chemistry,
Shandong University, Jinan 250100, P.R. China
e-mail: byx@sdu.edu.cn

Y. Wang

Department of Natural Science, Albany State University, Albany GA 31705, USA
e-mail: Yixuan.Wang@asurams.edu

2.1 Introduction

Since their discovery in 1991, [1] carbon nanotubes (CNTs) have attracted considerable interests in the field of nanotechnology due to their unique properties. Their high electrical conductivity and strength have made them promising materials for new applications such as field emitters [2] and scanning probes [3]. Single-walled carbon nanotubes (SWNTs) are π -bond aromatic molecules that can be either semi-conducting or metallic, depending on the helical angle and diameter [4]. Original simple considerations based on band structure of graphite lead to a conclusion that SWNT (n,m) is metallic for $n=m$, has a narrow band gap for $n-m=3k$ (integer k), and is a moderate-gap semiconductor otherwise [5]. The “ $n-m=3k$ ” rule was refined later by both theoretical and experimental studies [6].

CNTs are expected to be one of promising materials of the next-generation electronic devices, and they have already manifested their advantage as an efficient electron source through their excellent field-emission properties. Electrodes made from sheets of SWNTs have been demonstrated to actuate electromechanically in an electrochemical cell [7]. The redox chemistry of noncovalently functionalized SWNTs has received intensive attention [8]. For example, dispersion with polymers and surfactants such as proteins, DNA and sodium dodecyl sulfates (SDS) results in excellent SWNTs aqueous suspensions for redox chemistry studies [9]. Experimentalists have shown that SWNTs could be oxidized by strong oxidants such as KMnO_4 , and fully reduced by reductants such as NaBH_4 [8]. Extensive literatures exist on the subjects such as electronic structures, CNTs with defects, deformation and extra charges [8, 9e, 10]. Their electronic structures in the external electrical fields have also been theoretically discussed [10]. The properties of oxidative state of CNTs could affect the separation and enrichment process [11]. Recently theoretical calculations also showed that the injected charge could enhance the binding interaction between molecular hydrogen and fullerenes and CNTs [12]. Guo et al. reported that the electron injection was more effective in decreasing the energy barrier for the chemisorption of hydrogen molecules on armchair CNTs, while the hole injection was more effective for zigzag CNTs [13]. Luo et al. determined that fullerenes and CNTs have positive EAs, which was claimed to be related to the aggregation property of these carbon materials [14]. The electron affinity (EA) is defined as the total energy difference between the neutral and the negatively charged system, and the positive EA therefore implies that the neutral system has tendency to gain an electron and get reduced. Balbuena et al. reported the effect of nanotube length on the aromaticity of SWNTs [15].

SWNTs are also interesting to bioelectrochemistry. It is demonstrated that SWNTs could construct the nanostructured biointerfaces [16], enhance the electrochemistry reactivity and the electron transfer (ET) rates of biomolecules [17], considerably accumulate biomolecules [18], and assuage surface fouling effects [19]. SWNTs have also potential to prevent DNA from oxidation [20]. Due to the extensive applications mentioned above, the detailed understanding of the redox properties of the CNTs is very essential. However, the ionization potentials (IPs) and electron

affinities (EAs), two important indexes for field-emission and redox properties, seem to have been less examined. Herein, we report a comprehensive investigation of the size-dependences of IPs, EAs, and Mulliken electronegativity for three kinds of CNTs, armchair SWNT (n,n), zigzag SWNT (n,0) and DWNT (n,n) @ (n+5, n+5) on the basis of density functional theory analysis and calculation.

Electronic structures and activity distributions for H-passivated SWCNTs are not well defined, e.g., the ground state, and the variation of frontier molecular orbital with the size of the cluster. Besides the discussion of redox properties for the H-passivated SWCNTs, the electronic structures and frontier molecular orbitals were also discussed in the present chapter.

To provide biomedical implication of carbon nanotubes, ionization potentials of DNA bases (nucleic acid bases, NAB) with different DFT methods were provided at the end for a direct comparison with SWNTs, and the noncovalent interaction between a SWNT with guanine was visualized with reduced density gradient method [21]. As a comparison the interaction among C_{60} , $Li@C_{60}$ and NAB were also briefly reviewed.

2.2 Models and Methods

Generalized gradient approximation (GGA) type of density functional theory, Perdew and Wang's scheme (PW91) [22] with a double numerical plus polarization function (DNP), implemented in DMol³ of Material Studio 4.4 suite of program [23], was used to fully optimize the armchair and zigzag SWNT systems under periodic condition and calculate relevant properties. In order to ensure that the CNTs do not interact with their periodic images, supercell parameters, a and b (the sizes in the direction perpendicular to the nanotube axis) were defined by $a=b=D+25$ Å, as a function of the nanotube diameter D (D denotes the diameter of outer tube in the DWNTs). The parameter c (the size of the supercell along the nanotube axis) for armchair and zigzag SWNTs is 9.84 and 17.04 Å, respectively. The investigated SWNTs range from $n=3$ to 16 for (n,n) armchair and from 5 to 16 for (n,0) zigzag. The spin polarization scheme was applied to deal with open-shell systems. A $1*1*12$ Monkhorst-Pack k-point grid was used in the sampling of Brillouin zone, while $1*1*49$ k-point was used in the calculation of band gaps and Fermi energies. In the optimizations, the energy gradients and atomic displacements converged to within $1*10^{-5}$ Hartree/Bohr and $2*10^{-3}$ angstrom, respectively. The values of global orbital cutoff were set at 3.9 and 3.7 Å for anion systems and neutral systems, respectively. The same calculation method and parameters were applied to the DWNT systems. Due to the large system, only $1*1*8$ k-point setting is used in the optimization.

For an isolated system, the ionization potential is usually defined as $IP=E(N-1)-E(N)$, while the electron affinity is $EA=E(N)-E(N+1)$, where $E(N)$, $E(N+1)$, $E(N-1)$ are the total ground-state energies in the neutral (N), single negatively charged ($N+1$), and single positively charged ($N-1$) configurations,

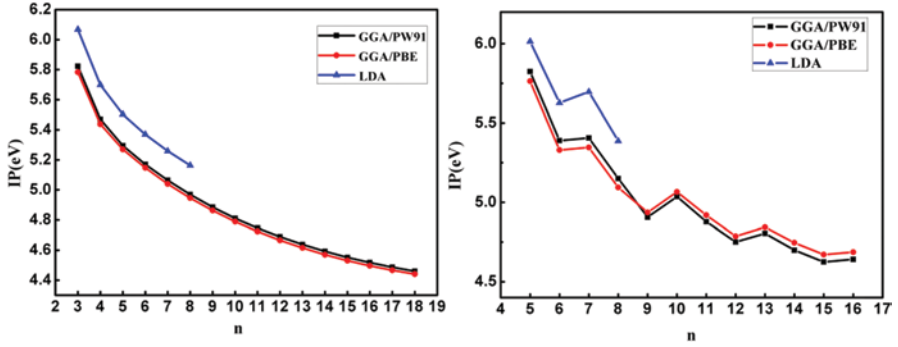


Fig. 2.1 Adiabatic ionization potential aIP of armchair (n,n) SWNTs (*left*) and zigzag (n,0) SWCNTs (*right*) as a function of n with different DFT methods

respectively. The definitions are also frequently employed to periodic systems [24]. For a periodic system, the electron affinity is estimated as $EA = E_{\text{vac}} - E_{\text{LUMO}}$ and the ionization potential as $IP = E_{\text{vac}} - E_{\text{HOMO}}$ (the vacuum energy E_{vac} is defined as the electrostatic potential energy in the vacuum, far away from the system) [25], and $WF = E_{\text{vac}} - (E_{\text{LUMO}} + E_{\text{HOMO}})/2$. Using all electron static and time-dependent DFT calculation, Zhou et al. reported that the IP decreases with the length of finite length (5,5) SWNT overall, exhibiting a periodicity [26]. The WFs of metallic and semiconducting SWNT's vs the inverse tube diameter $1/D$ vary in different ways, decrease in the former yet increase in the latter (WF was approximated as the negative Fermi energy $-E_F$, $E_{\text{vac}} \sim 0$) [27].

The GGA method of Perdew, Burke and Enzerhof's scheme [28] (PBE) and local density approximation (LDA) method were also used to calculate IP and EA values (as shown in Fig. 2.1), and a good agreement with those from PW91 was observed, validating the applied GFT method in the present work. LDA predicts higher IP than the GGA methods for both armchair and zigzag SWNTs.

To validate the calculation procedure, careful examinations for the employed scheme and parameters, such as the grid size for k-sampling, were also carried out and the results were shown in Fig. 2.2. For zigzag SWNTs, the adiabatic IP and EA with $1 \times 1 \times 8$ and $1 \times 1 \times 12$ k -point samplings are too close to be distinguished; for the armchair ones the results with the two large k -point samplings are rather close to each other. However, the results for all of cases with $1 \times 1 \times 2$ k -point are indeed far from those with the two large k -point samplings. Thus, $1 \times 1 \times 12$ Monkhorst-Pack k -point grid was used in the sampling of Brillouin zone.

As shown in Table 2.1, although Fermi levels (E_F) with $1 \times 1 \times 12$ and $1 \times 1 \times 49$ k -points are almost the same, energy gaps (E_g) with $1 \times 1 \times 49$ k -points are considerably improved especially for the armchair SWNTs. Thus the band gap needs much larger k -points to deal with than the Fermi level.

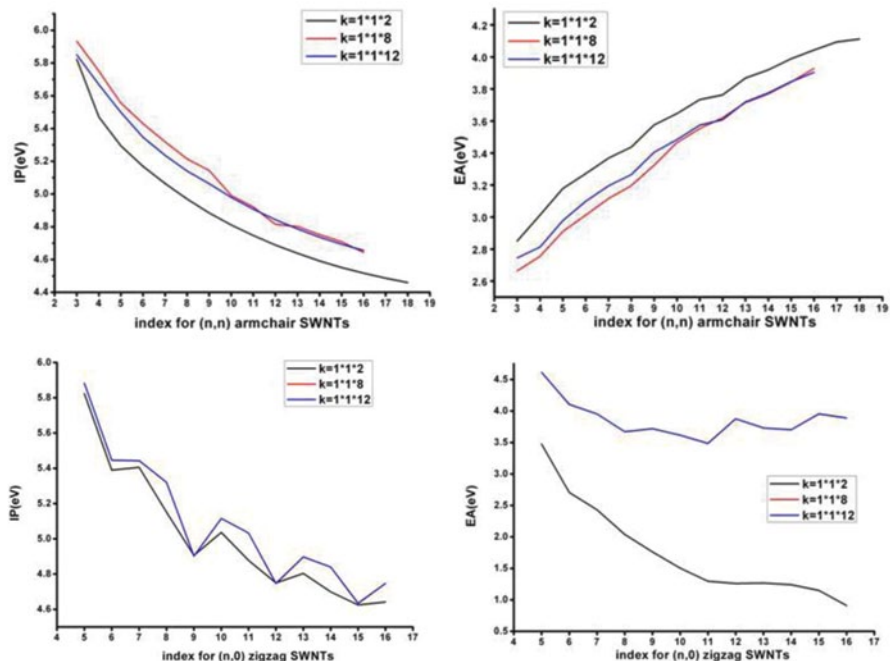


Fig. 2.2 Adiabatic ionization potential (aIP) and adiabatic electron affinity (aEA) of armchair (n,n) SWCNTs (*top*) and zigzag (n,0) SWCNTs (*bottom*) as a function of n with different k -point settings. For zigzag SWNTs, the $1*1*8$ and $1*1*12$ k -point settings are too close to be distinguished. Clearly, the $1*1*2$ is an ill-defined quantity

2.3 Results and Discussions

2.3.1 IP and EA of Armchair SWNT

The IP and EA estimated by the energy difference for armchair (n,n) SWNTs were collected in Table 2.2, and plotted against n in Fig. 2.3, respectively. Figure 2.3 shows that the adiabatic IPs for armchair (n,n) SWNTs decrease monotonically and smoothly with increasing SWNT diameters, whereas the adiabatic EAs monotonically increase. For the first few SWNTs from $n=3$ to 9 IPs drop rapidly by approximately 0.79 eV, and then IPs decrease gradually by only 0.33 eV from (10,10) to (16,16). The adiabatic EA has a similar change pattern with SWNTs to the IPs, e.g., EA increases from 2.75 for (3,3) to 3.40 eV for (9,9), and then is just increased by 0.42 eV from $n=10$ to 16. To the best of our knowledge, there are only few reports on IP and EA values of CNTs. In a similar periodic PBE type of DFT calculation to this work [24], the reported IPs for (5,5) SWNTs (60 atoms/cell) is 5.91 eV, which is in an excellent agreement with our result with the same model [5.98 eV for (5,5)–(60 atoms/cell)]. The work function (WF, $\sim -E_F$) has the same increase

Table 2.1 Calculated Fermi energy (E_f) and band gap E_g for (n,n) and (n,0) SWNTs at different k-point settings

(n,n)	k=1*1*12		k=1*1*49		(n,0)	k=1*1*12		k=1*1*49	
	E_f	E_g	E_f	E_g		E_f	E_g	E_f	E_g
n=3	-4.386	0.21	-4.391	0	n=5	-5.242	0.18	-5.242	0.17
4	-4.407	0.21	-4.414	0.02	6	-4.839	0	-4.839	0
5	-4.435	0.12	-4.432	0.05	7	-4.877	0.22	-4.875	0.21
6	-4.452	0.04	-4.452	0.06	8	-4.706	0.63	-4.707	0.62
7	-4.463	0.13	-4.464	0.03	9	-4.436	0.21	-4.436	0.13
8	-4.469	0.15	-4.469	0.05	10	-4.494	0.76	-4.494	0.73
9	-4.471	0.18	-4.472	0.06	11	-4.427	0.96	-4.427	0.95
10	-4.476	0.21	-4.476	0.03	12	-4.46	0.18	-4.46	0.08
11	-4.478	0.22	-4.472	0	13	-4.49	0.62	-4.49	0.59
12	-4.482	0.24	-4.484	0.03	14	-4.459	0.76	-4.459	0.74
13	-4.483	0.25	-4.483	0.01	15	-4.474	0.18	-4.473	0.06
14	-4.485	0.26	-4.484	0.02	16	-4.488	0.53	-4.488	0.5
15	-4.485	0.27	-4.488	0.03					
16	-4.487	0.27	-4.486	0.03					

Table 2.2 Calculated geometrical and electronic parameters for armchair SWCNT

(n,n)	D(Å) ^f	aIP ^b	vIP ^c	λ_h^d	aEA ^b	vEA ^c	λ_c^e	E_f	E_g
n=3	4.07	5.85	5.86	0.01	2.75	2.74	0.01	-4.391	0
4	5.42	5.67	5.67	0	2.81	2.81	0	-4.414	0.02
5	6.78	5.50	5.50	0	2.98	2.98	0	-4.432	0.05
6	8.14	5.35	5.36	0.01	3.10	3.09	0.01	-4.452	0.06
7	9.49	5.24	5.25	0.01	3.20	3.18	0.02	-4.464	0.03
8	10.85	5.14	5.14	0	3.27	3.26	0.01	-4.469	0.05
9	12.20	5.06	5.06	0	3.40	3.40	0	-4.472	0.06
10	13.56	4.98	4.98	0	3.48	3.48	0	-4.476	0.03
11	14.92	4.91	4.91	0	3.57	3.57	0	-4.472	0
12	16.27	4.84	4.84	0	3.61	3.61	0	-4.484	0.03
13	17.63	4.79	4.79	0	3.72	3.72	0	-4.483	0.01
14	18.98	4.74	4.74	0	3.77	3.77	0	-4.484	0.02
15	20.34	4.69	4.69	0	3.85	3.83	0.02	-4.488	0.03
16	21.70	4.66	4.66	0	3.90	3.90	0	-4.486	0.03

Fermi energy (E_f) and band gap (E_g)

^a all energies are in eV

^b adiabatic ionization potential (electron affinity)

^c vertical ionization potential (electron affinity)

^d hole reorganization energy

^e electron reorganization energy

^f diameter

trend as that for the metallic SWNTs [27]. The WF of 4.435 eV for the infinite (5,5) agrees very well with that of 4.37 eV predicted with all-electron method, and higher than that from plane-wave result of 4.28 eV [25].

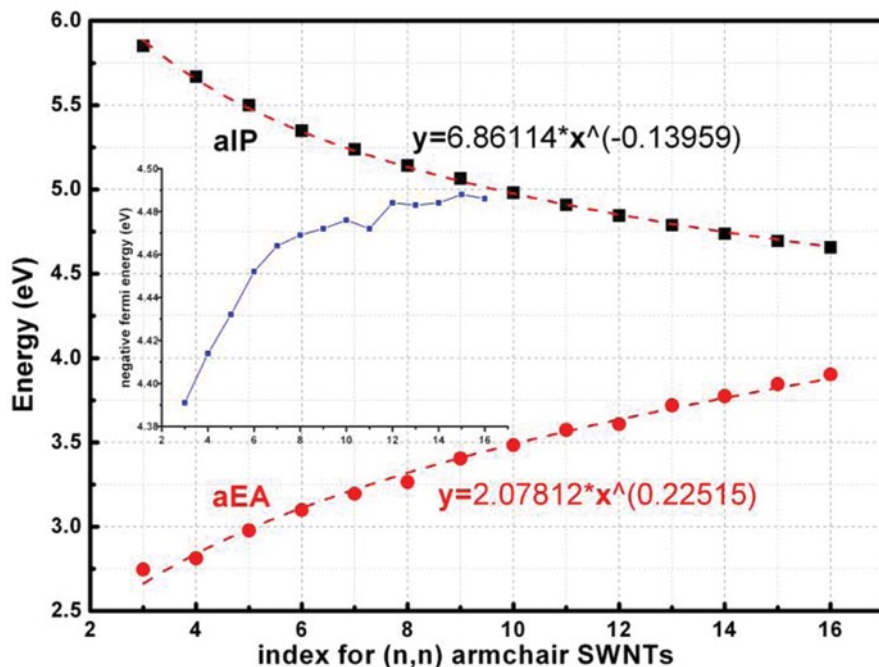


Fig. 2.3 Adiabatic ionization potentials (aIPs) and electron affinities (aEAs) of armchair SWNTs as a function of n , calculated with $IP = E(N-1) - E(N)$, and $EA = E(N) - E(N+1)$. The insert plot refers to the variation of negative Fermi energy (WF)

The difference between adiabatic IPs (EAs) and vertical IPs (EAs) are nonsignificant (as shown in Table 2.2), indicating that the hole reorganization energies (λ_h , the difference between the vertical IP and the adiabatic IP) and the electron reorganization energies (λ_e , the difference between the adiabatic EA and the vertical EA) for (n,n) SWNT are quite small. Generally, λ_e for an individual armchair SWNT is slightly larger than or equal to λ_h . This means that armchair SWNTs are more sensitive to an electron injection as compared with a hole injection.

The above results show that the thinner armchair SWNTs possess higher IP and lower EA, while the thicker ones possess lower IP and higher EA. Thus, the armchair SWNTs with small diameter do not tend to characterize either as an oxidant or a reductant, while the large diameter armchair SWNTs may be active as an oxidant as well as a reductant simultaneously. Regarding the application in redox chemistry, the (n,n) SWNTs with large diameter prefer to be both reduced and oxidized.

However, according to Fig. 2.4 both $IP \sim -E_{HOMO}$ and $EA \sim -E_{LUMO}$ show opposite trends to those shown in Fig. 2.3 although WFs remain the same trend. In the scheme of DMol³, the frontier molecular orbitals are predicted with only Gamma point, implying that the HOMO and LUMO actually refer to those for the truncated SWNT rather than periodic one. This is also the reason why the HOMO-LUMO gap is so significant, yet the band gaps for $k=1 \times 1 \times 49$ in Table 2.1 approach to zero. It is most likely that the IP and EA in Fig. 2.4 from the E_{HOMO} and E_{LUMO} represent

Fig. 2.4 Adiabatic ionization potentials (aIPs) and electron affinities (aEAs) of armchair SWNTs as a function of n , calculated with $EA = E_{\text{vac}} - E_{\text{LUMO}}$, $IP = E_{\text{vac}} - E_{\text{HOMO}}$, $WF = E_{\text{vac}} - (E_{\text{LUMO}} + E_{\text{HOMO}})/2$ (E_{vac} is approximated as zero)

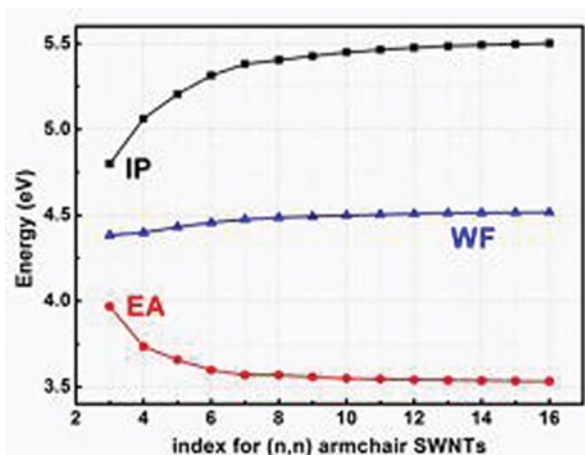
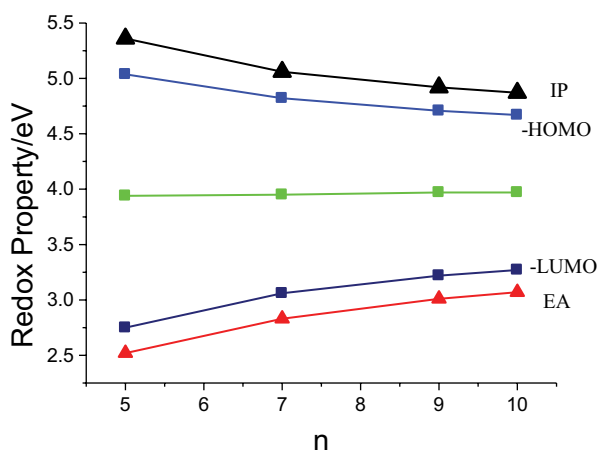


Fig. 2.5 Adiabatic ionization potentials ($IP = E(N-1) - E(N)$, black triangle), electron affinities ($EA = E(N) - E(N+1)$, red triangle), $-E_{\text{HOMO}}$, $-E_{\text{LUMO}}$, and Mulliken electronegativity χ (green) for H-passivated armchair (n,n) SWNTs (~ 22.2 Å in length) as a function of n



those of finite length SWNT without H-passivated. In addition, to solve convergence problem the occupation numbers are calculated by setting the occupation keyword at “thermal smearing” in DMol³ package, which uses a finite-temperature Fermi function to provide fractional occupation numbers [29]. Therefore, HOMO and LUMO were not well defined as well.

For a few H-passivated armchair SWNTs ($n = 5, 7, 9$ and 10) with approximated length of 22.2 Å (optimized with a hybrid GGA, M06-2X/6-31G*, implemented in Gaussian09 version B [30]) corresponding to 10 repeating units, IP, EA, -HOMO, and -LUMO are also evaluated, shown in Fig. 2.5. Similar to Fig. 2.3, the IP shows a decrease trend with the diameter, and the EA tends to increase with the diameter. These trends also agree with the variations of IP and EA with the length of H-passivated (5,5) SWNT [25]. In addition, $-E_{\text{HOMO}}$ and $-E_{\text{LUMO}}$ exhibit the same trends as IP and EA, respectively. The adiabatic IPs are approximately 0.2 – 0.3 eV higher than

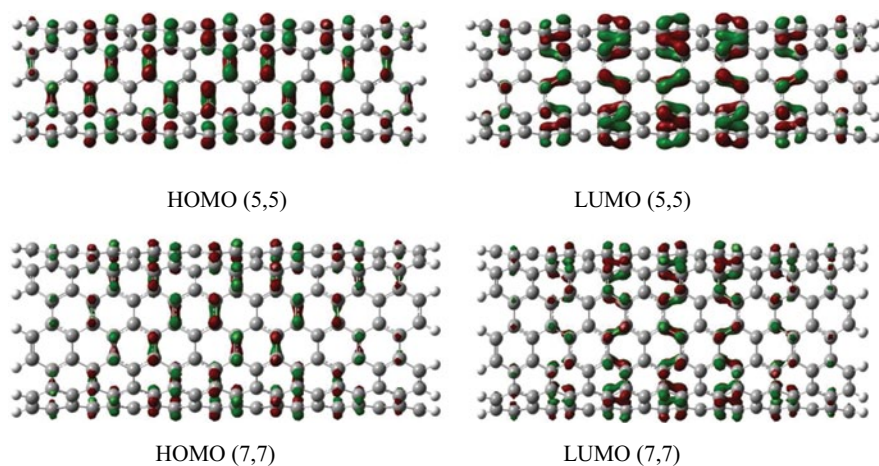
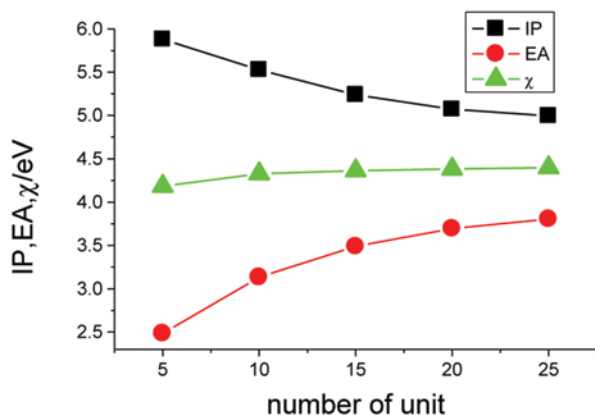


Fig. 2.6 The frontier orbitals for the H-passivated ~ 22 Å long armchair SWNT. (isovalue = 0.02 au)

Fig. 2.7 IP, EA and Mulliken electronegativity variation for H-passivated (5,5) SWNT ($C_{100}H_{20}-C_{500}H_{20}$) predicted with DFTB method

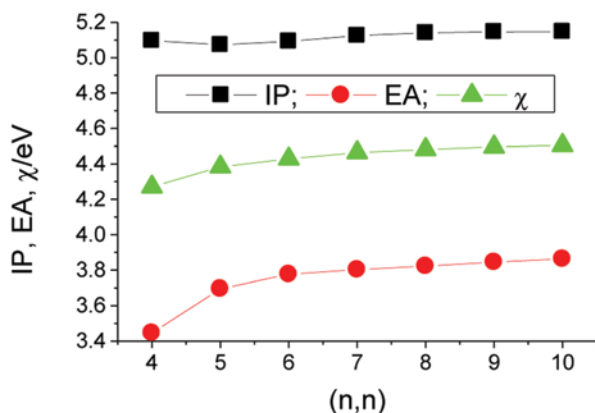


$-E_{\text{HOMO}}$, while the EAs are lower than $-E_{\text{LUMO}}$. The Mulliken electronegativity, the average of IP and EA only shows slightly increase with thickness of the SWNT.

To discuss the reaction activity of the H-passivated SWNT, the HOMO and LUMO for (5,5) and (7,7) are shown in Fig. 2.6. For both SWNTs the LUMOs dominantly spread over the inside carbons rather than the end carbons, while the carbons on the ends contribute a little to the HOMOs. The SWNT clusters in the length of 20 Å may be proper to simulate their chemical activity.

For the larger H-passivated armchair SWNTs (20 units, ~ 43 Å) the IP and EA were also estimated with DFTBA method that is a density-functional based tight-binding semi-empirical calculation, a method that is parametrized via the results of DFT calculations [31]. To validate the DFTB method, it was applied to H-passivated (5,5) SWNT for 5–25 units ($C_{100}-C_{500}H_{20}$). Compared with those for $C_{200}H_{20}$ from M06-2X/6-31G* in Fig. 2.5, the IP and EA shown in Fig. 2.7 are higher by

Fig. 2.8 IP, EA and Mulliken electronegativity variation for 20 units H-passivated (n,n) SWNT (~ 43 Å) predicted with DFTB method



0.17 and 0.61 eV, respectively. However, the general variation trend agree with that from Buonocore et al. [25].

The DFTB was then used to investigate the IP and EA for the H-passivated (n,n) SWNT (20 units, ~ 43 Å). The structures were fully optimized, and adiabatic IP and EA were then calculated. However, although EAs increase with the diameter of SWNTs as predicted with M06-2X for the short SWNTs (~ 22 Å in length), the adiabatic IPs in Fig. 2.8 do not significantly change. On the basis of the geometries from the DFTB method, the IPs and EAs will be estimated with more accurate DFT method, like GGA. It was worth to mention that the triplet states for the H-passivated (n,n) SWNT ($n=4,5$, and 6; 20 units) have higher energy than the singlet state with the DFTB method, implying that the ground state for H-passivated (n,n) SWNT is singlet state.

2.3.2 IPs and EAs of Zigzag SWNTs

The zigzag (n,0) tubes are predicted at the Hückel theory to be metallic or nearly metallic when n is a multiple of 3, and semiconductors for the rest. Adiabatic IPs and EAs for zigzag (n,0) SWNTs were shown in Fig. 2.9. It can be seen that similar to the cases of armchair SWNTs the adiabatic IPs for (n,0) SWNTs also generally decrease with diameter, but obviously there are a few local increases occurring just after $n=3k$, exhibiting a steplike pattern. This can be attributed to the well-known fact that $(3k, 0)$ SWNTs behave like metals usually having low IPs. Figure 2.9 shows that the IP of (9,0) is smaller than those of (7,0) and (8,0) SWNTs, i.e., (9,0) SWNT can easily donate an electron as compared with (7,0) and (8,0) SWNTs, which agrees with the conclusion in a recent report [32]. Table 2.3 indicates that the applied PW91 does predict rather small band gaps for $(3k, 0)$ zigzag, 0.0, 0.13, 0.08, and 0.06 eV for $k=2-5$, which are comparable to those from the hybrid DFT B3LYP [33]. It is interesting to note that the above step like feature of IPs is periodic, or exhibits a group behavior. Such a group behavior is somehow characterized by the IPs for SWNTs with $n=3k$ ($k=2-6$) as compared with their neighbors, $(n-1, 0)$ and

Design and Applications of Nanomaterials for Sensors

Seminario, J.M. (Ed.)

2014, X, 290 p. 150 illus., 50 illus. in color., Hardcover

ISBN: 978-94-017-8847-2